

CMM-SolMech 2022

Modeling of the Influence of Elevated Temperature on Oxygen Distribution in Soft Tissue

Marek JASIŃSKI* , Maria ZADON 

*Department of Computational Mechanics and Engineering
Silesian University of Technology*

Gliwice, Poland; e-mail: maria.zadon@polsl.pl

*Corresponding Author e-mail: marek.jasinski@polsl.pl

The purpose of the study was to analyze the combined model of bioheat transfer and oxygen distribution in tissue during exposition to the external heat impulse. The effect of temperature and thermal damage to the tissue on the values of its thermophysical parameters was taken into account. The variable value of the perfusion coefficient affects the blood velocity in the capillary and thus the distribution of the partial oxygen pressure in the tissue. Various models of the oxygen dissociation curves were also considered and a sensitivity analysis was performed for the parameters of the oxygen distribution model. In the numerical realization stage, the finite difference method and the shooting method were used.

Keywords: bioheat transfer; tissue thermal damage; oxygen transport; Krogh cylinder; oxy-hemoglobin dissociation curve; finite difference method; shooting method; sensitivity analysis.

1. INTRODUCTION

Thermal damage to biological tissue is a complex process that involves numerous changes in the tissue domain. Under the influence of an uncontrolled external heat impulse, the values of the thermophysical parameters of the tissue can change. Special attention should be paid to the perfusion coefficient, which describes the presence of blood in the tissue and is often taken as a certain indicator of thermal damage. It is known that blood vessels dilate under the influence of heat, but if the thermal pulse is prolonged and/or the temperature is high enough, they can undergo permanent damage resulting in a decrease in perfusion. It should be noted that in the smallest blood vessels, the capillaries, gas exchange takes place to supply oxygen to the tissue. In view of this, an increase in tissue temperature can cause a disruption of this process, and thus the hypoxia phenomenon [1–5].

The amount of oxygen delivered to the tissue under normal conditions depends on the oxygen content in the blood. It can take two forms: chemical bonds that form oxyhemoglobin and free molecules. The concentration of these free molecules is described by oxygen partial pressure. When the partial pressure decreases, oxyhemoglobin releases oxygen, and reverse reactions are also possible. The relationship between oxygen hemoglobin saturation and oxygen partial pressure is described by a sigmoidal oxyhemoglobin dissociation curve (ODC). It is laboratory-determined for specific temperature values, carbon dioxide, pH, 2,3-DPG (2,3 diphosphoglycerate), and other substances. Note that an increase in temperature shifts the dissociation curve to the right, which is called the Bohr effect [6–12].

Mathematical models describing the presence of oxygen in biological tissue are various and often derived from the concept of the Krogh cylinder, which represents a cylindrical region of tissue around a capillary. This model, despite the initial numerous simplifications adopted by its author, became the basis for many subsequent works related to various therapies, muscle work during exercise, the presence of cancerous tissue in the body, or the process of angiogenesis, among others [7, 8, 10, 13, 14]. On the mathematical side, the model is described by differential equations for the tissue and capillary subdomains, in which the dependent variable is the partial oxygen pressure. These equations are supplemented by equations related, for example, to the saturation of oxyhemoglobin in the capillary area, and the connecting element between the two types of equations is the adopted ODC model [10, 13, 14].

To analyze heat distribution in biological tissue, one of the existing bioheat transfer equations is used. The oldest of them, but still the most popular, is the Pennes equation, in which the presence of small blood vessels and metabolic phenomena is taken into account through appropriate source heat functions [4, 14–17]. The Cattaneo-Vernotte equation (hyperbolic thermal wave model) takes into account the relaxation time, i.e., the delay of the heat flux with respect to the temperature gradient [18]. In the dual-phase lag model derived from the theory of porous media, a thermalization time was additionally introduced to denote the delay in the temperature gradient caused by heat conduction in microscale structures [19–25].

The bioheat transfer equations are sometimes supplemented by various functions for thermophysical parameters, allowing us to take into account their alteration depending on the temperature and/or the degree of thermal damage to the tissue. In turn, thermal damage is most often expressed by an Arrhenius model assuming an irreversible exponential increase in thermal damage as a function of temperature [4, 14, 16]. Recent work on the use of this model postulates the inclusion of the effect of oxygen as a counteracting factor to thermal damage [26].

The analysis carried out in this paper consists of steps related to bioheat transfer analysis, estimation of tissue thermal damage, and oxygen distribution in tissue. The 3D domain of a biological tissue subjected to an external thermal impulse is taken into consideration. The analysis is based on the bioheat transport equation in the Pennes form. Using the Arrhenius scheme, the degree of thermal damage to the tissue is estimated, and, tissue parameters are treated as temperature- or damage-dependent. The thermal model is supplemented by an axisymmetric Krogh cylinder model to analyze changes in the partial pressure of oxygen in the capillary vessel and surrounding tissue. The main equation in this model for the tissue subdomain includes a component related to oxygen consumption in the tissue, while the equation for the capillary subdomain takes into account blood saturation and its relationship to partial oxygen pressure via three models of the oxygen dissociation curve. In addition, a sensitivity analysis of the parameters appearing in the equation for the tissue subdomain, i.e., Krogh coefficient and oxygen demand, was carried out. The oxygen distribution model is linked to the thermal model through the relationship between blood velocity in the capillary and the perfusion coefficient. In the numerical realization stage, mainly a finite difference method is used; the shooting method was used to determine the distribution of oxygen in the tissue subdomain.

2. GOVERNING EQUATIONS

In Fig. 1, the models considered in the current work are presented. On the left, the considered domain of 3D biological tissue for thermal analysis is presented. The tissue domain is exposed to the external heat impulse at the upper Γ_0 boundary. On the right, the model for considering oxygen transport in tissue is visible. The main assumption of the Krogh model is that tissue is composed of contiguous cylindrical units (the so-called Krogh cylinders), with a diameter of the individual cylinders large enough that there is no oxygen transport between them [5, 7, 8]. The Krogh cylinder corresponds to the tissue surrounding the capillary vessel, but its dimensions are much smaller compared to the cube

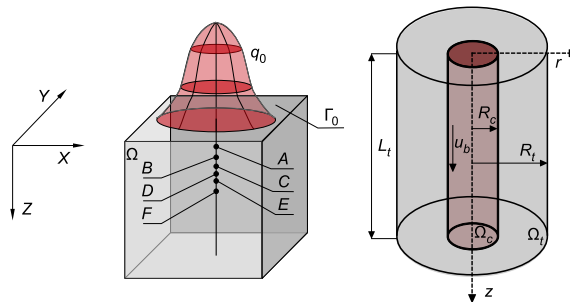


FIG. 1. Domains considered for the bioheat transfer and oxygen distribution model.

that forms the bioheat transfer model (this paper adopts: $1.5 \times 1.5 \times 1.5$ cm for the bioheat transfer model, $R_c = 2.5 \mu\text{m}$, $R_t = 25 \mu\text{m}$, $L_t = 500 \mu\text{m}$ for the Krogh cylinder), and the overall model proposed in the paper can be treated as a multiscale problem. Due to differences in the dimensions of the two models, the full capillary structure is not considered but rather a single Krogh cylinder [5, 10].

In the bioheat transfer model, the presence of blood is described by a perfusion coefficient. In practice, it is determined, among other things, by knowing the number of capillaries in the cross-section or the tissue volume (depending on the method adopted). Thus, it is also possible to determine the velocity of blood in the capillary u_b based on knowledge of the perfusion coefficient and dimensions of the capillary. This relationship was used to combine the bioheat transfer model and the oxygen distribution model. In the bioheat transfer model, points A – F have been highlighted, for which the curves of the determined parameters, including the perfusion coefficient, will be presented. For selected time steps, calculations will be carried out using the oxygen distribution model.

The bioheat transfer in the tissue domain Ω is described by the Pennes equation supplemented with appropriate boundary and initial conditions [4, 16, 17]:

$$\begin{aligned}
 \mathbf{x} \in \Omega : \quad & c\dot{T} = \nabla(\lambda\nabla T) + Q_{\text{perf}} + Q_{\text{met}}, \\
 \mathbf{x} \in \Gamma_0 : \quad & q = q_0, \quad \text{for } t \leq t_{\text{exp}}, \quad q = 0, \quad \text{for } t > t_{\text{exp}}, \\
 \mathbf{x} \in \Gamma_c : \quad & q = 0, \\
 t = 0 : \quad & T = T_{\text{init}},
 \end{aligned}
 \tag{2.1}$$

where λ [$\text{W} \cdot \text{m}^{-1} \cdot \text{K}^{-1}$] is the thermal conductivity, c [$\text{J} \cdot \text{m}^{-3} \cdot \text{K}^{-1}$] is the volumetric specific heat of tissue and blood, respectively, Q_{met} [$\text{W} \cdot \text{m}^{-3}$] is the metabolic heat source, q_0 [$\text{W} \cdot \text{m}^{-2}$] is the boundary heat flux, t_{exp} [s] is the exposure time while T_{init} denotes the initial distribution of temperature. The external heat impulse at the boundary Γ_0 is described by a function:

$$q_0(x, y) = q_{0,\text{max}} \exp\left(-\frac{2(x^2 + y^2)}{r_{\text{imp}}^2}\right),
 \tag{2.2}$$

where $q_{0,\text{max}}$ [$\text{W} \cdot \text{m}^{-2}$] denotes the maximal value of the heat flux, while r_{imp} is the radius of the impulse. The function of internal heat sources associated with perfusion Q_{perf} is as follows [4, 16]:

$$Q_{\text{perf}}(\mathbf{x}, t) = c_B w [T_B - T(\mathbf{x}, t)],
 \tag{2.3}$$

where c_B [$\text{J} \cdot \text{m}^{-3} \cdot \text{K}^{-1}$] is the volumetric specific heat of the blood, T_B corresponds to the arterial blood temperature, and w [s^{-1}] is the perfusion coefficient.

Tissue subjected to an external heat impulse can undergo thermal damage. The basic model for determining the degree of thermal damage to tissue is the Arrhenius scheme [16]:

$$(2.4) \quad \text{Arr}(\mathbf{x}, t^F) = \int_0^{t^F} A \exp \left[-\frac{E}{RT(\mathbf{x}, t)} \right] dt,$$

where R [$\text{J} \cdot \text{mol}^{-1} \cdot \text{K}^{-1}$] is the universal gas constant, E [$\text{J} \cdot \text{mol}^{-1}$] is the activation energy, and A [s^{-1}] is the preexponential factor. The integral values of $\text{Arr} = 1$ and $\text{Arr} = 4.6$ correspond to a probability of 63% and 99% of cell death at a specific point \mathbf{x} , respectively. Both values are used as criteria for tissue necrosis.

It is obvious that thermally damaged tissue can damage the blood vessel network within it. Therefore, the perfusion coefficient w was assumed using a function that maps the phenomena that occur in the tissue during the increase in temperature (the initial increase in perfusion during vasodilation) and the subsequent thermal damage (the decrease in perfusion resulting from rupture of the vasculature) as (w_0 is the initial perfusion coefficient) [1, 4, 14]:

$$(2.5) \quad w(\text{Arr}) = \begin{cases} (1 + 25\text{Arr} - 260\text{Arr}^2) w_0, & 0 \leq \text{Arr} \leq 0.1, \\ (1 - \text{Arr}) w_0, & 0.1 < \text{Arr} \leq 1, \\ 0, & \text{Arr} > 1. \end{cases}$$

Other thermophysical parameters of the tissue may also change as a result of an increase in its temperature. In the current work, the thermal conductivity λ is assumed to be temperature-dependent (temperature in Kelvin), whereas the volumetric specific heat c is treated as dependent on thermal conductivity. The following functions are assumed for these reasons [27, 28]:

$$(2.6) \quad \lambda(T) = 0.6489 + 0.0427 \arctan [0.0252(T - 315.314)],$$

$$(2.7) \quad c(\lambda) = (3.385\lambda + 2.17) \cdot 10^6.$$

Separate equations for the radial and axial directions are applied for the Krogh cylinder model (see Fig. 1). For radial direction [4, 5, 14]:

$$(2.8) \quad \begin{aligned} r \in \Omega_t : \quad K_t \frac{1}{r} \frac{d}{dr} \left(r \frac{dP_t}{dr} \right) &= M_t(P_t), \quad M_t(P_t) = \frac{M_0 P_t}{P_{\text{crit}} + P_t}, \\ r = R_c : \quad 2\pi R_c K_t \frac{dP_t}{dr} &= -k(P_b - P_t), \\ r = R_t : \quad \frac{dP_t}{dr} &= 0, \end{aligned}$$

where P_t and P_b [mmHg] are the partial oxygen pressure in tissue and blood, respectively, K_t [$(\text{cm}^2 \cdot \text{s}^{-1})(\text{mol} \cdot \text{cm}^{-3} \cdot \text{mmHg}^{-1})$] is the Krogh diffusion coef-

ficient, M_0 [$\text{mol} \cdot \text{cm}^{-3} \cdot \text{s}^{-1}$] is the oxygen demand, P_{crit} [mmHg] is the partial pressure that corresponds to half maximum oxygen consumption, and k [$(\text{cm}^2 \cdot \text{s}^{-1})(\text{mol} \cdot \text{cm}^{-3} \cdot \text{mmHg}^{-1})$] is the mass transfer coefficient. Note that component $M_t(P_t)$ is oxygen consumption in the tissue, which in current work is assumed to be the Michaelis-Menten kinetics.

Along the Krogh cylinder, the partial pressure of oxygen in the capillary P_b changes, which is expressed by the following relation [29]:

$$(2.9) \quad \begin{aligned} z \in \Omega_c : \quad Q_b \kappa_b \frac{d[S_{\text{Hb}}(P_b)]}{dz} &= -k(P_b - P_t), \\ z = 0 : \quad P_b &= P_{b \text{inlet}}, \end{aligned}$$

where Q_b [$\text{cm}^3 \cdot \text{s}^{-1}$] denotes the blood flow rate in the capillary, κ_b [$\text{mol} \cdot \text{cm}^{-3}_{\text{blood}}$] is the oxygen carrying capacity of blood at 100% saturation, while S_{Hb} is the saturation of oxyhemoglobin, determined by the adopted model of oxyhemoglobin dissociation curve (ODC).

The bioheat transfer model and the oxygen distribution model are linked through parameters related to blood flow: the perfusion coefficient w and the blood velocity in the capillary u_b . Because the perfusion coefficient is dependent on the Arrhenius integral, the blood velocity in the capillary varies with the thermal damage [14, 29]

$$(2.10) \quad w = \frac{Q_b}{\pi R_t^2 L_t} = \frac{\pi R_c^2 u_b}{\pi R_t^2 L_t} \quad \rightarrow \quad u_b = w(\text{Arr}) L_t \frac{R_t^2}{R_c^2}.$$

As already mentioned, Eq. (2.9) should be supplemented by the ODC model. The most popular ODC model is Hill's model in the form of (Fig. 2) [10, 11, 29]:

$$(2.11) \quad S_{\text{Hb}}(P_b) = \frac{P_b^n}{P_b^n + P_{50}^n},$$

where n denotes the Hill coefficient related to the slope of the dissociation curve, while P_{50} is the oxygen pressure corresponding to 50% hemoglobin saturation.

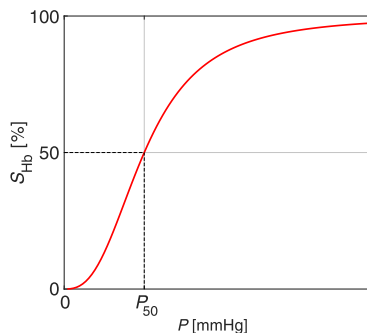


FIG. 2. Oxyhemoglobin dissociation curve with parameters of the Hill model.

The popularity of Hill’s model is mainly due its simplicity and the ease of obtaining the inverse relationship $P_b(S_{Hb})$. However, it is assumed that the model reproduces well the relationship between partial pressure and saturation only in the range of 20–80%, which may be important for modeling phenomena associated with thermal damage to biological tissue. For this reason, in addition to the Hill model, the ODC models proposed by Adair were considered in the study [7]:

$$\begin{aligned}
 (2.12) \quad S_{Hb}(P_b) &= \frac{a_1 P_b + 2a_2 P_b^2 + 3a_3 P_b^3 + 4a_4 P_b^4}{4(1 + a_1 P_b + a_2 P_b^2 + a_3 P_b^3 + a_4 P_b^4)}, \\
 a_1 &= 0.02567, & a_2 &= 0.00077734, \\
 a_3 &= 0.00000447, & a_4 &= 0.000002251,
 \end{aligned}$$

as well as the ODC model proposed by Kelman [13]:

$$\begin{aligned}
 (2.13) \quad P_b < 12 \text{ mmHg} : \quad & S_{Hb}(P_b) = b_1 P_b + b_2 P_b^2, \\
 P_b \geq 12 \text{ mmHg} : \quad & S_{Hb}(P_b) = \frac{a_1 P_b + a_2 P_b^2 + a_3 P_b^3 + P_b^4}{4(a_4 + a_5 P_b + a_6 P_b^2 + a_7 P_b^3 + P_b^4)}, \\
 a_1 &= -8532.2289, & a_2 &= 2121.401, \\
 a_3 &= -67.073989, & a_4 &= 935960.87, \\
 a_5 &= -31346.258, & a_6 &= -2396.1674 \\
 a_7 &= -67.104406, \\
 b_1 &= 0.003683, & b_2 &= 0.000584.
 \end{aligned}$$

In Fig. 3, the scheme shows the relationship between the particular parts of the current analysis. The thermal analysis uses thermophysical parameters

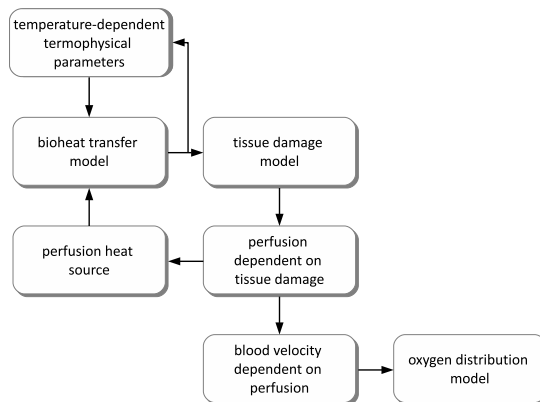


FIG. 3. Data transfer between particular parts of the model considered.

that are updated with each temperature change. One can see that after tissue damage is evaluated, the perfusion coefficient is updated, and then these new values are used in the next step of the analysis. The blood velocity is calculated on the basis of the perfusion coefficient, and then the value is used in the oxygen distribution model. In thermal analysis, the transient model is considered, while the oxygen model is used for the steady-state problem. This means that the oxygen distribution model was calculated only for some selected time steps.

3. SENSITIVITY ANALYSIS

Parameters in biological systems are often very different, which may be due to individual characteristics, among other things. One way to account for such differences is to use sensitivity analysis. The literature on various methods of sensitivity analysis in bioheat transfer problems is quite extensive [30–34]. In the current work, the direct method was used to investigate the sensitivity of the oxygen transport model to a change in the Krogh coefficient K_t and the oxygen demand M_0 . Note that the sensitivity analysis was performed under the assumption that $w = w_0$, which corresponds to thermally intact tissue.

Taking as $p_s = K_t, M_0$ ($s = 1, 2$) and differentiating the Eq. (2.8) due to p_s :

$$(3.1) \quad \frac{\partial}{\partial p_s} \left[K_t \frac{1}{r} \frac{dP_t}{dr} + K_t \frac{d^2P_t}{dr^2} \right] = \frac{\partial}{\partial p_s} [M_t(P_t)],$$

so

$$(3.2) \quad \frac{\partial K_t}{\partial p_s} \frac{d^2P_t}{dr^2} + K_t \frac{\partial}{\partial p_s} \left(\frac{d^2P_t}{dr^2} \right) + \frac{1}{r} \frac{\partial K_t}{\partial p_s} \frac{dP_t}{dr} + \frac{1}{r} K_t \frac{\partial}{\partial p_s} \left(\frac{dP_t}{dr} \right) = \frac{\partial M_t(P_t)}{\partial p_s}.$$

By performing the appropriate mathematical transformations and taking into account that

$$(3.3) \quad \frac{d^2P_t}{dr^2} = \frac{M_t(P_t)}{K_t} - \frac{1}{r} \frac{dP_t}{dr}$$

one obtains an equation in the form

$$(3.4) \quad K_t \frac{d^2}{dr^2} \left(\frac{\partial P_t}{\partial p_s} \right) + K_t \frac{1}{r} \frac{d}{dr} \left(\frac{\partial P_t}{\partial p_s} \right) = \frac{\partial M_t(P_t)}{\partial p_s} - \frac{\partial K_t}{\partial p_s} \frac{M_t(P_t)}{K_t}.$$

We assume that

$$(3.5) \quad U_s = \frac{\partial P_t}{\partial p_s}$$

is a function of the sensitivity of the parameters p_s , so finally, we can write the equation as follows:

$$(3.6) \quad K_t \frac{1}{r} \frac{d}{dr} \left[r \frac{dU_s}{dr} \right] = \frac{\partial M_t(P_t)}{\partial p_s} - \frac{\partial K_t}{\partial p_s} \frac{M_t(P_t)}{K_t},$$

$$\frac{\partial M_t}{\partial p_s} = \frac{\frac{\partial M_0}{\partial p_s} P_{\text{crit}} P_t + \frac{\partial M_0}{\partial p_s} P_t^2 + M_0 P_{\text{crit}} U_s}{(P_{\text{crit}} + P_t)^2}$$

along with boundary conditions obtained in a similar manner

$$(3.7) \quad r = R_c : \quad 2\pi R_c K_t \frac{dU_s}{dr} = -k \left[U_s + \frac{1}{K_t} \frac{\partial K_t}{\partial p_s} (P_b - P_t) \right],$$

$$r = R_t : \quad \frac{dU_s}{dr} = 0.$$

4. METHODS OF SOLUTION

In the stage of numerical implementation, an explicit scheme of the finite difference method was used to solve the bioheat transfer problem and shooting methods to solve the task of oxygen distribution and associated sensitivity analysis tasks.

The finite difference method uses the 7-point stencil shown in Fig. 4, with corresponding definitions of differential quotients (h is the grid step) [35, 36]

$$(4.1) \quad \left(\lambda \frac{\partial T}{\partial x} \right)_{i+0.5,j,k}^{f-1} = \lambda_{01} \frac{T_1^{f-1} - T_0^{f-1}}{h}, \quad \left(\lambda \frac{\partial T}{\partial x} \right)_{i-0.5,j,k}^{f-1} = \lambda_{02} \frac{T_0^{f-1} - T_2^{f-1}}{h},$$

$$\left(\lambda \frac{\partial T}{\partial y} \right)_{i,j+0.5,k}^{f-1} = \lambda_{03} \frac{T_3^{f-1} - T_0^{f-1}}{h}, \quad \left(\lambda \frac{\partial T}{\partial y} \right)_{i,j-0.5,k}^{f-1} = \lambda_{04} \frac{T_0^{f-1} - T_4^{f-1}}{h},$$

$$\left(\lambda \frac{\partial T}{\partial z} \right)_{i,j,k+0.5}^{f-1} = \lambda_{05} \frac{T_5^{f-1} - T_0^{f-1}}{h}, \quad \left(\lambda \frac{\partial T}{\partial z} \right)_{i,j,k-0.5}^{f-1} = \lambda_{06} \frac{T_0^{f-1} - T_6^{f-1}}{h},$$

where

$$(4.2) \quad \lambda_{0e} = \frac{2\lambda_0\lambda_e}{\lambda_0 + \lambda_e}, \quad i = 1, \dots, 6.$$

So, for the central node, one can write

$$(4.3) \quad \nabla (\lambda \nabla T) = \left[\frac{\partial}{\partial x} \left(\lambda \frac{\partial T}{\partial x} \right)_0^{f-1} + \frac{\partial}{\partial y} \left(\lambda \frac{\partial T}{\partial y} \right)_0^{f-1} + \frac{\partial}{\partial z} \left(\lambda \frac{\partial T}{\partial z} \right)_0^{f-1} \right]$$

$$= \frac{1}{h} \sum_{e=1}^6 \lambda_{0e} \left(T_e^{f-1} - T_0^{f-1} \right).$$

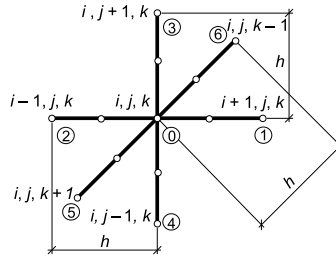


FIG. 4. The 7-point stencil used in the bioheat transfer problem.

The final equation for the central node of the stencil can be written in the form

$$(4.4) \quad T_0^f = T_0^{f-1} + \frac{\Delta t}{ch} \sum_{e=1}^6 \lambda_{0e} (T_e^{f-1} - T_0^{f-1}) + \frac{c_B w \Delta t}{c} (T_B - T_0^{f-1}) + \frac{\Delta t}{c} Q_{\text{met}}.$$

The solving equations for the boundary nodes are obtained in a similar manner.

As already mentioned, the shooting method was used to determine the partial pressure in the tissue subdomain Ω_t of the Krogh cylinder model (Eq. (2.8)). This method was also used in sensitivity analysis tasks to determine the sensitivity function U_s for the parameters K_t (Krogh coefficient) and M_0 (oxygen demand) (Eqs. (3.5)–(3.6)).

The idea of a shooting method is to transform a boundary value problem into an initial value problem (IVP). The boundary condition at the selected boundary of the domain under consideration is then used as the initial condition, while the second initial condition must be guessed. The task defined this way can then be solved using one of the numerical methods for solving ODEs. The obtained value of the solution “on the second boundary” of the domain must be compared with the given boundary condition there. If the accuracy between the value of the boundary condition and the obtained from IVP is unsatisfactory, the initial value is guessed again and the problem is solved once again. The procedure is repeated until the value of the IVP solution agrees with the value of the boundary condition “on the second boundary”. It should be added that approximate methods of solving equations are used to determine the guess values [37–39].

One can write governing equations with boundary conditions for the oxygen distribution problem (Eq. (2.8)) and sensitivity analysis tasks (3.5)–(3.6) in a more general form

$$(4.5) \quad \begin{aligned} r \in \Omega_t : \quad & K_t \frac{1}{r} \frac{d}{dr} \left(r \frac{dV}{dr} \right) = Q_V, \\ r = R_c : \quad & \frac{dV}{dr} + e_1 V = e_2, \\ r = R_t : \quad & \frac{dV}{dr} = e_3, \end{aligned}$$

where V stands for P_t or the corresponding sensitivity function U_s , and taking as the boundary from which the shots are taken $r = R_t$, the initial-value problem can be written as

$$\begin{aligned}
 (4.6) \quad & K_t V'' + K_t \frac{1}{r} V' = Q_V, \\
 & V'(R_t) = e_3, \\
 & V(R_t) = \alpha_{\text{guess}}.
 \end{aligned}$$

After finding the solution of IVP, the following difference is checked

$$(4.7) \quad r(R_c, \alpha_{\text{guess}}) = V'(R_c, \alpha_{\text{guess}}) + e_1 V(R_c, \alpha_{\text{guess}}) - e_2.$$

The calculations of the shooting method were carried out in the Matlab 2021b environment. In the oxygen distribution problem, the secant method was used for the determination of the guess value and the fourth-order Runge-Kutta method, while for sensitivity problems (Eqs. (3.5) and (3.6)), the combination of built-in solvers `fzero` and `ode45` was used [37].

5. RESULTS OF COMPUTATIONS

In this work, a cube-shaped tissue domain with dimensions of $1.5 \times 1.5 \times 1.5$ cm was considered. To reduce the computational complexity, only a quarter of the area was taken into account, so in the end, the calculations were carried out on the dimension of the tissue of $0.75 \times 0.75 \times 1.5$ cm. For the FDM analysis, the domain was discretized using $76 \times 76 \times 151$ nodes. The following values of the thermophysical parameters of tissue and blood were assumed: $c_B = 3.9962 \text{ MJ} \cdot \text{m}^{-3} \cdot \text{K}^{-1}$, $w_0 = 0.041 \text{ s}^{-1}$, $Q_{\text{met}} = 245 \text{ W} \cdot \text{m}^{-3}$, and $T_B = 37^\circ\text{C}$. Values used in the boundary-initial condition for the thermal problem were: $q_{0,\text{max}} = 19000 \text{ W} \cdot \text{m}^{-2}$, $t_{\text{exp}} = 20 \text{ s}$, and $T_{\text{init}} = 37^\circ\text{C}$. For the model that uses Arrhenius integral, the following data were assumed: $A = 3.1 \cdot 10^{98} \text{ s}^{-1}$, $E = 6.27 \cdot 10^5 \text{ J} \cdot \text{mol}^{-1}$, and $R = 8.314 \text{ J} \cdot \text{mol}^{-1} \cdot \text{K}^{-1}$ [4, 31, 40].

The calculations for the oxygen distribution model were carried out for the following data: $R_c = 2.5 \text{ }\mu\text{m}$, $R_t = 25 \text{ }\mu\text{m}$, $L_t = 500 \text{ }\mu\text{m}$, $K_t = 2.202 \cdot 10^{-14} (\text{cm}^2 \cdot \text{s}^{-1})(\text{mol} \cdot \text{cm}^{-3} \cdot \text{mmHg}^{-1})$, $M_0 = 5.000 \cdot 10^{-8} \text{ mol} \cdot \text{cm}^{-3} \cdot \text{s}^{-1}$, $P_{\text{crit}} = 1 \text{ mmHg}$, $k = 2.79 \cdot 10^{-13} (\text{cm}^2 \cdot \text{s}^{-1})(\text{mol} \cdot \text{cm}^{-3} \cdot \text{mmHg}^{-1})$, $P_{\text{binlet}} = 100 \text{ mmHg}$, $\kappa_b = 9.1 \cdot 10^{-6} \text{ mol} \cdot \text{cm}^{-3}_{\text{blood}}$, $n = 2.57$, and $P_{50} = 27 \text{ mmHg}$ [4, 13, 29].

In the first step, the task related to determining the temperature distribution, tissue damage, and damage-dependent perfusion coefficient was solved. Then the values determined in this task for the selected node were used to solve tasks related to oxygen distribution.

Figure 5 shows the temperature distribution in the domain under consideration for 10, 20 and 30 s, while Fig. 6 shows the distribution of the Arrhenius integral and perfusion coefficient for the same time steps. It can be seen that the Arrhenius integral exceeds both values of the necrosis criteria, i.e., $Arr > 1$ and $Arr > 4.6$. For the perfusion coefficient, both the areas of increased perfusion, above $w_0 = 0.041 \text{ s}^{-1}$, and the area where, due to exceeding $Arr > 1$, the perfusion disappeared (see Eq. (2.5)) are clearly visible.

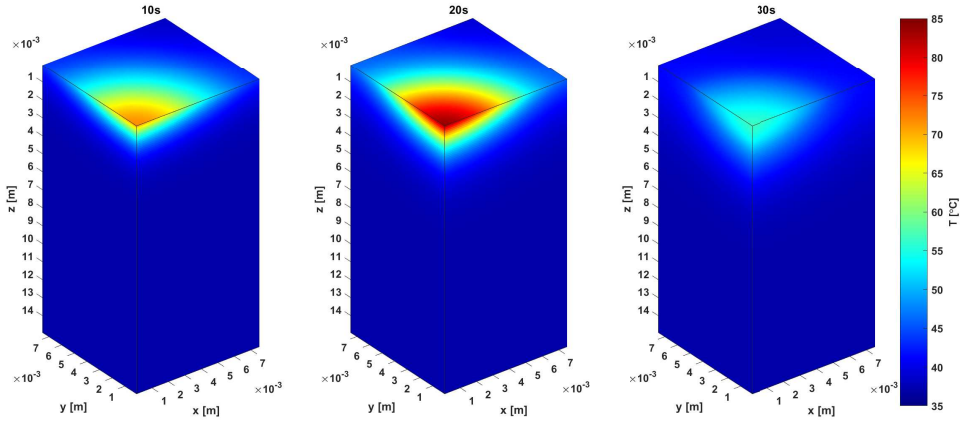


FIG. 5. Distribution of temperature for 10, 20, and 30 s.

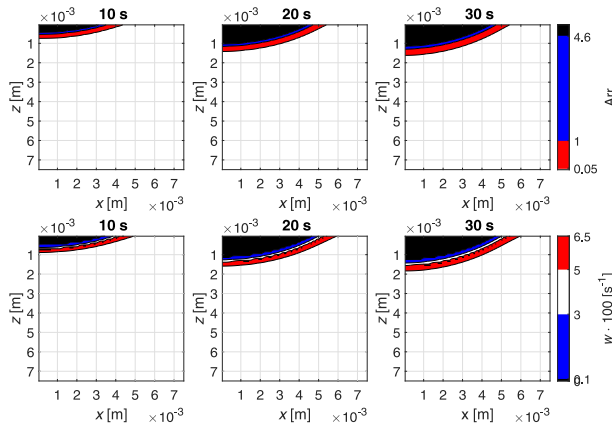


FIG. 6. Distribution of the Arrhenius integral and perfusion coefficient for 10, 20 and 30 s.

Figures 7 and 8 are also related to the bioheat transfer analysis. Figure 7 presents courses of temperature and Arrhenius integral at selected points of the domain (see Fig. 1). The coordinates of the particular nodes are as follows [cm]:

$A(0.75, 0.75, 0.005)$, $B(0.75, 0.75, 0.293)$, $C(0.75, 0.75, 0.412)$, $D(0.75, 0.75, 0.472)$, $E(0.75, 0.75, 0.492)$, and $F(0.75, 0.75, 0.641)$. Figure 8 shows, among other things, the history of perfusion and temperature at point D . This point was chosen as the one where the Krogh cylinder oxygen distribution model is placed. As the temperature increases, the perfusion also increases, which is associated with the phenomenon of vasodilation of blood vessels. A further increase in temperature causes more and more tissue destruction; this leads to the disappearance of perfusion. The maximum perfusion value $w = 0.0656 \text{ s}^{-1}$ at this point was reached for time $t = 12.45 \text{ s}$.

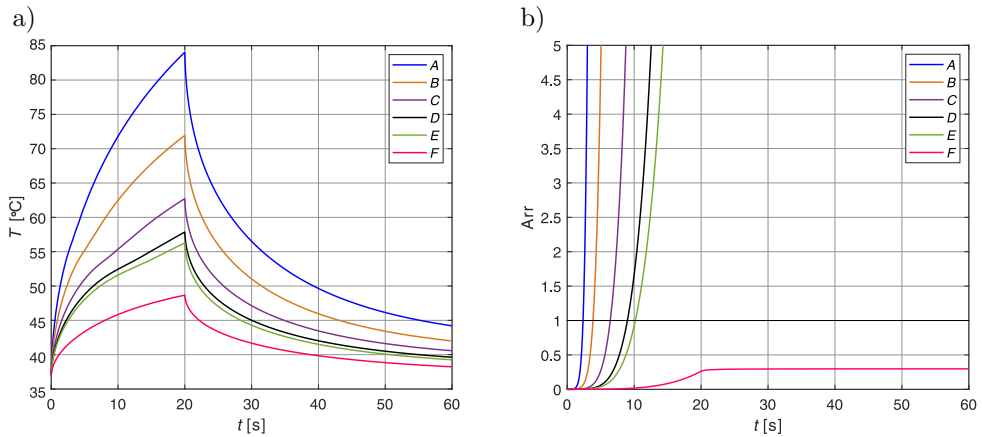


FIG. 7. Courses of temperature (a) and Arrhenius integral (b) at selected nodes.

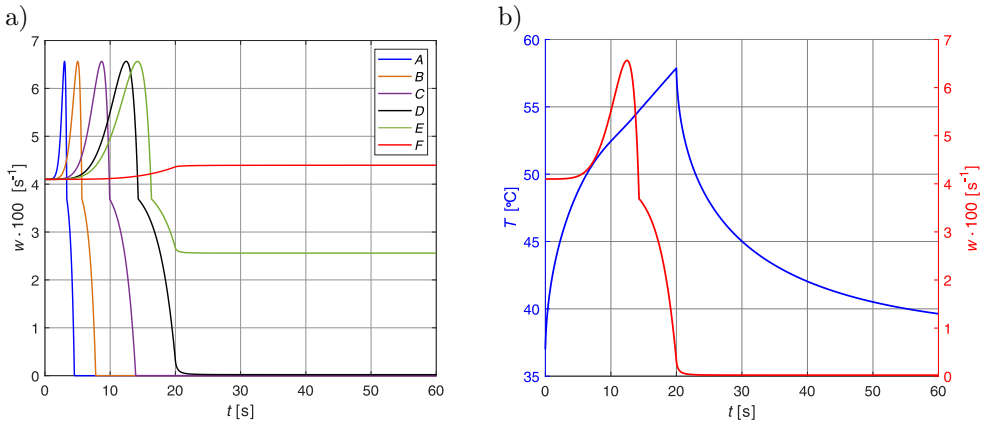


FIG. 8. Courses of the perfusion coefficient in selected nodes (a) and history of perfusion and temperature at node D (b).

To analyze oxygen distribution, it is necessary to know the blood velocity in the capillary u_b (see Eq. (2.10)). This was calculated from the value of the perfusion coefficient at node D .

Figure 9 shows the results of the calculations for the Krogh cylinder model in the radial (Eq. (2.8)) and axial (Eq. (2.9)). Calculations were made for selected time steps, using various models of oxyhemoglobin dissociation curve, that is, Hill, Adair, and Kelman models (see Eqs. (2.11)–(2.13)). For the radial direction, the results shown correspond to $z = 0$ and $z = L_t/2$. As you can see, in most cases, the results for different ODCs are quite close to each other. The exceptions are the curves obtained for the axial direction for 20 s, according to which, for Kelman ODC, hypoxia occurs earlier than for the other two curves.

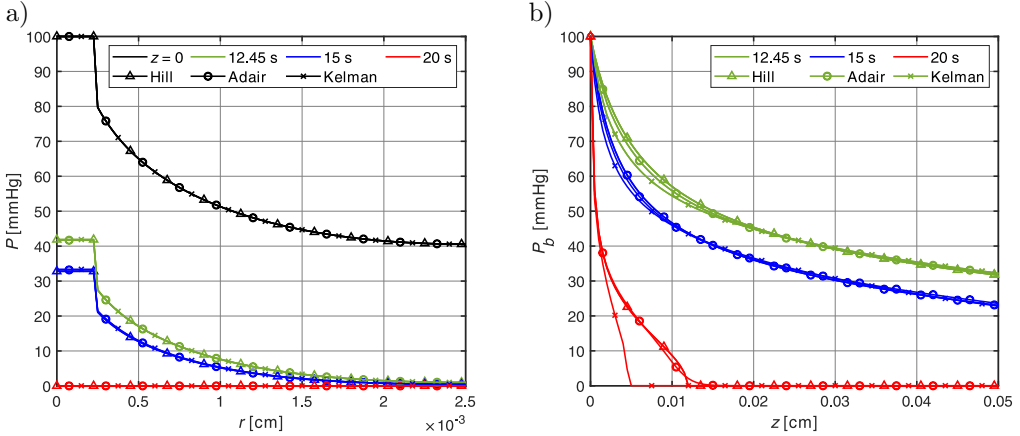


FIG. 9. Distribution of the partial pressure in radial (a) and axial (b) directions for selected time steps.

Figure 10 shows the partial pressure in the whole Krogh cylinder, while Table 1 shows the percentage of tissue area in which hypoxia occurred. The

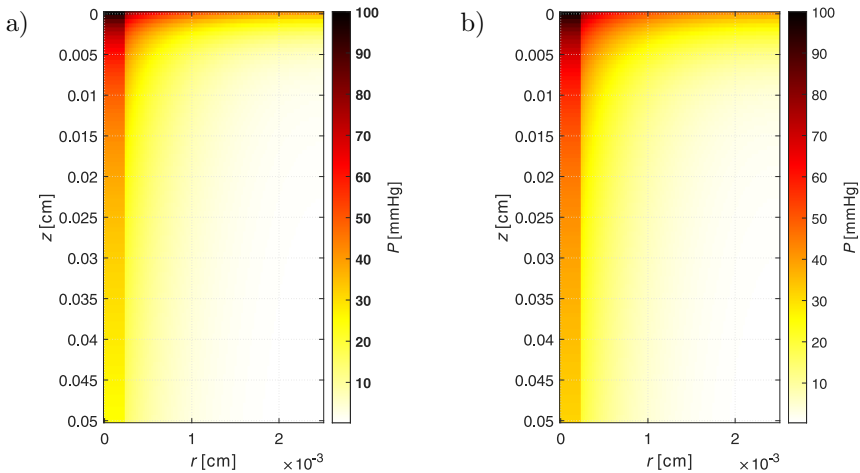


FIG. 10. Distribution of the partial oxygen pressure in Krogh cylinder for 0 s (a) and 12.45 s (b) (Hill ODC).

Table 1. Hypoxia volume in tissue subdomain for selected time steps.

	Hill	Adair	Kelman
10 s	13.45%	13.24%	12.97%
12.45 s	10.29%	10.18%	9.83%
15 s	21.51%	21.13%	21.15%
20 s	86.66%	86.49%	97.58%

volume of hypoxia was calculated for the subdomain of tissue; it was assumed that the tissue is hypoxic if $P_t < 1$ mmHg.

The last part of the results is related to the sensitivity analysis. Figure 11 shows the sensitivity functions for the Krogh coefficient (U_1) and oxygen demand (U_2) for $z = 0$ and $z = L_t/2$, while Fig. 12 presents the functions multiplied by $\Delta p_s = (\pm 5\%, \pm 10\%) \cdot p_s$ for $z = 0$.

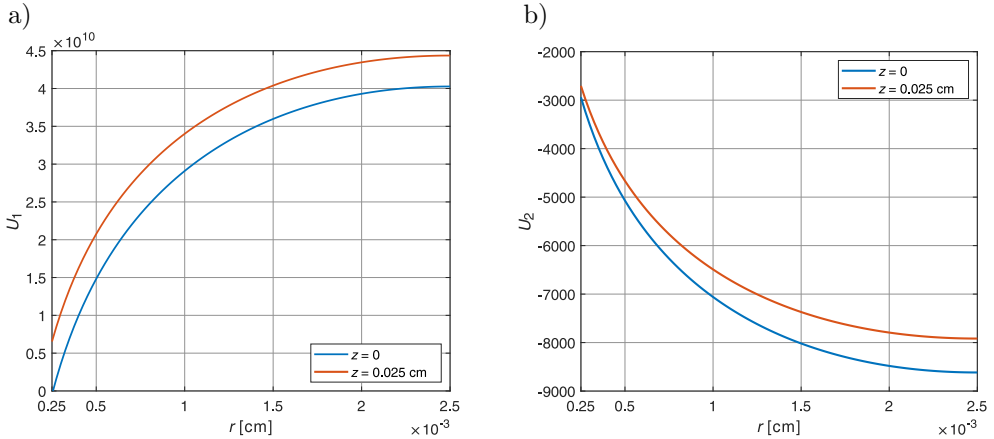


FIG. 11. Sensitivity functions: a) for the Krogh coefficient (U_1), b) for the oxygen demand (U_2).

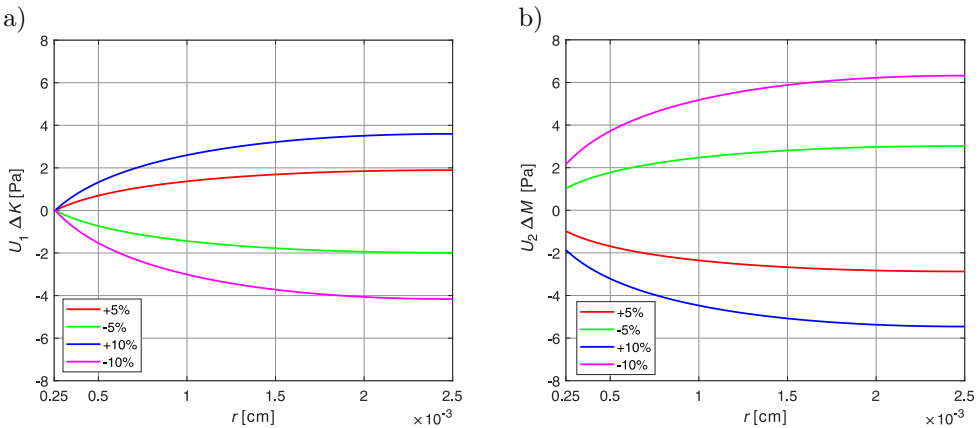


FIG. 12. Sensitivity functions expressed as $U_s \cdot \Delta p_s$ for $\Delta p_s = (\pm 5\%, \pm 10\%) \cdot p_s$.

6. FINAL REMARKS

As the results of the calculations show, the phenomena that occur under the influence of an external heat impulse affect the distribution of oxygen in the tissue. Exceeding the necrosis criterion for the Arrhenius integral (Arr) sequentially results in the disappearance of perfusion resulting from the adopted function (Eq. (2.5)), a decrease in blood velocity in the capillary (Eq. (2.10)), and, ultimately, the occurrence of hypoxia. In addition, the choice of the oxyhemoglobin dissociation curve (ODC) model may be important, especially in the low oxygen partial pressure range (Fig. 9). Note that this curve changes shape under the influence of temperature: it shifts to the right when the temperature increases (Bohr effect). The current work does not take this phenomenon into account. Although the phenomenon has been known in the literature, there is not very much data on the problem, especially on ODC models other than Hill's model [4, 7, 11, 29].

Also included in the results presented are the sensitivity functions for the Krogh coefficient K_t and oxygen demand M_0 for the oxygen distribution model (Figs. 11 and 12). As one can see, for a 10% change in parameter values, they can cause changes of about ± 4 mmHg for the Krogh coefficient and ± 5 mmHg for the oxygen demand. Sensitivity functions were determined for $w = w_0$, which corresponds to the normothermic state. In the case of progressive thermal damage to the tissue, these increases can significantly affect the depth of hypoxia occurrence.

It should be added that the calculations associated with the sensitivity analysis were compared with those taking into account the parameter increments in the model (Eq. (2.8)), and the differences between the results obtained were small. This demonstrates the fairly good accuracy resulting from the shooting method used [37].

The overall model presented shows that the phenomenon of thermal damage is complex, not limited to one type of phenomena. In addition, there are suggestions in the literature about the effect of oxygen on some kind of reversal of the thermal damage phenomenon, which may be important, especially when modeling various types of therapies in which the temperatures used are not high. Attempts have been made to account for this phenomenon by attaching an additional component to the Arrhenius integral [26].

The presence of oxygen in the tissue is also important for the photochemical phenomena that occur in the tissue during the photodynamic therapy treatment. The temperature increases achieved with this therapy are not high (except for some variants of PDT), but they can affect changes in perfusion and thus the concentration of triplet oxygen in the tissue. This form reacts with the photosensitizer, eventually turning into singlet oxygen, which is cytotoxic to cancerous

tissues. Oxygen supply values are estimated in PDT-related models based on the Krogh cylinder [9, 10, 41].

The model presented here does not exhaust the issue of modeling thermal damage, taking into account changes in the thermophysical parameters of the tissue and the distribution of oxygen in the tissue. In the future, the newer bioheat transfer equation, which is the dual-phase lag model, should be included in this type of model in particular. One of its bases is the division of tissue into so-called equivalent circles that take into account the area of tissue around a blood vessel. In light of the structure of the Krogh model, this offers interesting interpretive possibilities. Other types of connection between bioheat and oxygen distribution models, such as the aforementioned Bohr effect, would also need to be considered. Furthermore, conducting a more accurate sensitivity analysis for these models will undoubtedly bring them closer to the real conditions that occur during thermal damage.

ACKNOWLEDGMENTS

The research was funded from the projects of the Silesian University of Technology, Faculty of Mechanical Engineering.

REFERENCES

1. ABRAHAM J.P., SPARROW E.M., A thermal-ablation bioheat model including liquid-to-vapor phase change, pressure- and necrosis-dependent perfusion, and moisture-dependent properties, *International Journal of Heat and Mass Transfer*, **50**(13–14): 2537–2544, 2007, doi: 10.1016/J.IJHEATMASSTRANSFER.2006.11.045.
2. HASSANPOUR S., SABOONCHI A., Modeling of heat transfer in a vascular tissue-like medium during an interstitial hyperthermia process, *Journal of Thermal Biology*, **62**, Part B: 150–158, 2016, doi: 10.1016/J.JTHERBIO.2016.06.022.
3. AFRIN N., ZHOU J., ZHANG Y., TZOU D.Y., CHEN J.K., Numerical simulation of thermal damage to living biological tissues induced by laser irradiation based on a generalized dual phase lag model, *Numerical Heat Transfer Applications, Part A: Applications*, **61**(7): 483–501, 2012, doi: 10.1080/10407782.2012.667648.
4. JASIŃSKI M., Numerical analysis of the temperature impact to the oxygen distribution in the biological tissue, *Journal of Applied Mathematics and Computational Mechanics*, **19**(3): 17–28, 2020, doi: 10.17512/JAMCM.2020.3.02.
5. HE Y., SHIRAZAKI M., LIU H., HIMENO R., SUN Z., A numerical coupling model to analyze the blood flow, temperature, and oxygen transport in human breast tumor under laser irradiation, *Computers in Biology and Medicine*, **36**(12): 1336–1350, 2006, doi: 10.1016/J.COMPBIOMED.2005.08.004.
6. FRY B.C., ROY T.K., SECOMB T.W., Capillary recruitment in a theoretical model for blood flow regulation in heterogeneous microvessel networks, *Physiological Reports*, **1**(3): e00050, 2013, doi: 10.1002/PHY2.50.

7. GOLDMAN D., Theoretical models of microvascular oxygen transport to tissue, *Microcirculation*, **15**(8): 795–811, 2008, doi: 10.1080/10739680801938289.
8. SECOMB T.W., ALBERDING J.P., HSU R., DEWHIRST M.W., PRIES A.R., Angiogenesis: An adaptive dynamic biological patterning problem, *PLoS Computational Biology*, **9**(3): e1002983, 2013, doi: 10.1371/JOURNAL.PCBI.1002983.
9. ZHU T.C., KIM M.M., LIANG X., FINLAY J.C., BUSCH T.M., In-vivo singlet oxygen threshold doses for PDT, *Photonics and Lasers in Medicine*, **4**(1): 59–71, 2015, doi: 10.1515/PLM-2014-0037.
10. ZHU T.C., LIU B., PENJWEINI R., Study of tissue oxygen supply rate in a macroscopic photodynamic therapy singlet oxygen model, *Journal of Biomedical Optics*, **20**(3): 038001, 2015, doi: 10.1117/1.JBO.20.3.038001.
11. HLASTALA M.P., WOODSON R.D., WRANNE B., Influence of temperature on hemoglobin-ligand interaction in whole blood, *Journal of Applied Physiology*, **43**(3): 545–550, 1977, doi: 10.1152/JAPPL.1977.43.3.545.
12. CASTAING M., SINET M., Temperature and oxygenation of human blood at constant total CO₂ content, *Pflügers Archiv, European Journal of Physiology*, **386**(2): 135–140, 1980, doi: 10.1007/BF00584200.
13. WHITELEY J.P., GAVAGHAN D.J., HAHN C.E.W., Mathematical modelling of oxygen transport to tissue, *Journal of Mathematical Biology*, **44**: 503–522, 2002, doi: 10.1007/S002850200135.
14. JASIŃSKI M., Numerical analysis of thermal damage and oxygen distribution in laser irradiated tissue, *Journal of Applied Mathematics and Computational Mechanics*, **21**(2): 51–62, 2022, doi: 10.17512/JAMCM.2022.2.05.
15. EL-NABULSI R.A., ANUKOOL W., Nonlocal thermal effects on biological tissues and tumors, *Thermal Science and Engineering Progress*, **34**: 101424, 2022, doi: 10.1016/J.TSEP.2022.101424.
16. PARUCH M., Mathematical modeling of breast tumor destruction using fast heating during radiofrequency ablation, *Materials (Basel, Switzerland)*, **13**(1): 136, 2020, doi: 10.3390/MA13010136.
17. MOCHNACKI B., CIESIELSKI M., Sensitivity of transient temperature field in domain of forearm insulated by protective clothing with respect to perturbations of external boundary heat flux, *Bulletin of the Polish Academy of Sciences: Technical Sciences*, **64**(3): 591–598, 2016, doi: 10.1515/BPASTS-2016-0066.
18. EL-NABULSI R.A., Fractal Pennes and Cattaneo–Vernotte bioheat equations from product-like fractal geometry and their implications on cells in the presence of tumour growth, *Journal of the Royal Society Interface*, **18**(182): 20210564, 2021, doi: 10.1098/RSIF.2021.0564.
19. CHAUDHARY R.K., KUMAR D., RAI K.N., SINGH J., Analysis of thermal injuries using classical Fourier and DPL models for multi-layer of skin under different boundary conditions, *International Journal of Biomathematics*, **14**(6): 2150040, 2021, doi: 10.1142/S1793524521500406.
20. CHAUDHARY R.K., KUMAR D., RAI K.N., SINGH J., Numerical simulation of the skin tissue subjected to hyperthermia treatment using a nonlinear DPL model, *Thermal Science and Engineering Progress*, **34**: 101394, 2022, doi: 10.1016/J.TSEP.2022.101394.

21. MAJCHRZAK E., TURCHAN L., DZIATKIEWICZ J., Modeling of skin tissue heating using the generalized dual phase-lag equation, *Archives of Mechanics*, **67**(6): 417–437, 2015, doi: 10.24423/AOM.1777.
22. SAEED T., ABBAS I., Finite element analyses of nonlinear DPL bioheat model in spherical tissues using experimental data, *Mechanics Based Design of Structures and Machines*, **50**(4): 1287–1297, 2022, doi: 10.1080/15397734.2020.1749068.
23. ALZHRANI F., ABBAS I., A numerical solution of nonlinear DPL bioheat model in biological tissue due to laser irradiations, *Indian Journal of Physics*, **96**(2): 377–383, 2022, doi: 10.1007/s12648-020-01988-w.
24. AKULA S.C., MANIYERI R., Numerical simulation of bioheat transfer: a comparative study on hyperbolic and parabolic heat conduction, *Journal of the Brazilian Society of Mechanical Sciences and Engineering*, **42**(62): 1–13, 2020, doi: 10.1007/s40430-019-2132-x.
25. MAJCHRZAK E., STRYCYŃSKI M., Dual-phase lag model of heat transfer between blood vessel and biological tissue, *Mathematical Biosciences and Engineering: MBE*, **18**(2): 1573–1589, 2021, doi: 10.3934/MBE.2021081.
26. DOMBROVSKY L.A., Laser-induced thermal treatment of superficial human tumors: An advanced heating strategy and non-Arrhenius law for living tissues, *Frontiers in Thermal Engineering*, **1**: 807083, 2022, doi: 10.3389/FTHER.2021.807083.
27. ODEN J.T., DILLER K.R., BAJAJ C., BROWNE J.C., HAZLE J., BABUŠKA I., BASS J., BIDUAT L., DEMKOWICZ L., ELLIOTT A., FENG Y., FUENTES D., PRUDHOMME S., RYLANDER M.N., STAFFORD R.J., ZHANG Y., Dynamic data-driven finite element models for laser treatment of cancer, *Numerical Methods for Partial Differential Equations*, **23**(4): 904–922, 2007, doi: 10.1002/NUM.20251.
28. HAMILTON G., *Investigations of the Thermal Properties of Human and Animal Tissues*, Ph. D. Thesis, University of Glasgow, UK, 1998.
29. MCGUIRE B.J., SECOMB T.W., A theoretical model for oxygen transport in skeletal muscle under conditions of high oxygen demand, *Journal of Applied Physiology*, **91**(5): 2255–2265, 2001, doi: 10.1152/jappl.2001.91.5.2255.
30. MAJCHRZAK E., KAŁUŻA G., Sensitivity analysis of temperature in heated soft tissues with respect to time delays, *Continuum Mechanics and Thermodynamics*, **34**(2): 587–599, 2021, doi: 10.1007/s00161-021-01075-3.
31. MAJCHRZAK E., TURCHAN L., JASIŃSKI M., Identification of laser intensity assuring the destruction of target region of biological tissue using the gradient method and generalized dual-phase lag equation, *Iranian Journal of Science and Technology – Transactions of Mechanical Engineering*, **43**: 539–548, 2019, doi: 10.1007/s40997-018-0225-2.
32. JASIŃSKI M., Modelling of tissue thermal injury formation process with application of direct sensitivity method, *Journal of Theoretical and Applied Mechanics*, **52**(4): 947–957, 2014, doi: 10.15632/JTAM-PL.52.4.947.
33. DAVIES C.R., SAIDEL G.M., HARASAKI H., Sensitivity analysis of one-dimensional heat transfer in tissue with temperature-dependent perfusion, *Journal of Biomechanical Engineering*, **119**(1): 77–80, 1997, doi: 10.1115/1.2796068.
34. MAJCHRZAK E., KAŁUŻA G., Sensitivity analysis of biological tissue freezing process with respect to the radius of spherical cryoprobe, *Journal of Theoretical and Applied Mechanics*, **44**(2): 381–392, 2006.

35. MOCHNACKI B., PIASECKA BELKHAYAT A., Numerical modeling of skin tissue heating using the interval finite difference method, *Molecular & Cellular Biomechanics*, **10**(3): 233–244, 2013, doi: 10.3970/MCB.2013.010.233.
36. MAJCHRZAK E., MOCHNACKI B., Dual-phase lag equation. Stability conditions of a numerical algorithm based on the explicit scheme of the finite difference method, *Journal of Applied Mathematics and Computational Mechanics*, **15**(3): 89–96, 2016, doi: 10.17512/JAMCM.2016.3.09.
37. KESKIN A.Ü., *Boundary Value Problems for Engineers*, Springer International Publishing, Heidelberg, 2019, doi: 10.1007/978-3-030-21080-9.
38. ATILI B.S., SYAM M.I., Efficient shooting method for solving two point boundary value problems, *Chaos, Solitons & Fractals*, **35**(5): 895–903, 2008, doi: 10.1016/J.CHAOS.2006.05.094.
39. HA S.N., A nonlinear shooting method for two-point boundary value problems, *Computers & Mathematics with Applications*, **42**(10–11): 1411–1420, 2001, doi: 10.1016/S0898-1221(01)00250-4.
40. KORCZAK A., JASIŃSKI M., Modelling of biological tissue damage process with application of interval arithmetic, *Journal of Theoretical and Applied Mechanics*, **57**(1): 249–261, 2019, doi: 10.15632/JTAM-PL.57.1.249.
41. JASIŃSKI M., ZADOŃ M., Mathematical modeling of the phenomena that occur in a biological tissue containing a photosensitizer, *Journal of Applied Mathematics and Computational Mechanics*, **21**(4): 40–51, 2022, doi: 10.17512/jamcm.2022.4.04.

Received December 20, 2022; accepted version March 3, 2023.



Copyright © 2023 The Author(s).

This is an open-access article distributed under the terms of the Creative Commons Attribution-ShareAlike 4.0 International ([CC BY-SA 4.0 https://creativecommons.org/licenses/by-sa/4.0/](https://creativecommons.org/licenses/by-sa/4.0/)) which permits use, distribution, and reproduction in any medium, provided that the article is properly cited. In any case of remix, adapt, or build upon the material, the modified material must be licensed under identical terms.